Fibrin-Dextran Hydrogels with Tunable Porosity and Mechanical Properties

pubs.acs.org/Biomac

Article

Fibrin–Dextran Hydrogels with Tunable Porosity and Mechanical Properties

Shannon Anna Jung,[▽] Hanna Malyaran,[▽] Dan Eugen Demco, Anna Manukanc, Leonie Sophie Häser, Vytautas Kučikas, Marc van Zandvoort, Sabine Neuss,* and Andrij Pich*

Cite This: *Biomacromolecules* 2023, 24, 3972–3984

Read Online

ACCESS | Metrics & More | Article Recommendations | Supporting Information

ABSTRACT: Hydrogels as scaffolds in tissue engineering have gained increasing attention in recent years. Natural hydrogels, e.g., collagen or fibrin, are limited by their weak mechanical properties and fast degradation, whereas synthetic hydrogels face issues with biocompatibility and biodegradation. Therefore, combining natural and synthetic polymers to design hydrogels with tunable mechanical stability and cell affinity for biomedical applications is of interest. By using fibrin with its excellent cell compatibility and dextran with controllable mechanical properties, a novel bio-based hydrogel can be formed. Here, we synthesized fibrin and dextran-methacrylate (MA)-based hydrogels with tailorable mechanical properties, controllable degradation, variable pore sizes, and ability to support cell proliferation. The hydrogels are formed through in situ gelation of fibrinogen and dextran-MA with thrombin and dithiothreitol. Swelling and nuclear magnetic resonance diffusometry measurements showed that the water uptake and mesh sizes of fabricated hydrogels decrease with increasing dextran-MA concentrations. Cell viability tests confirm that these hydrogels exhibit no cytotoxic effect.

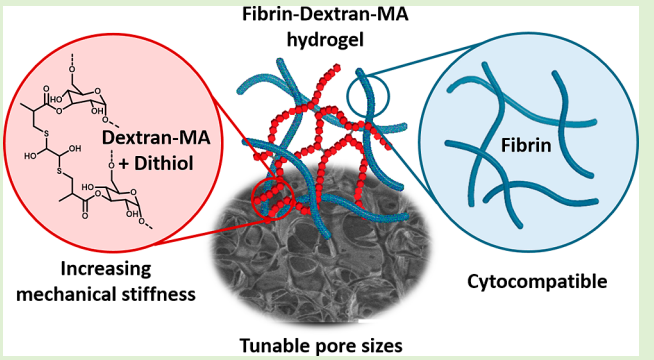

1. INTRODUCTION

The concept of tissue engineering (TE) is based on three components: scaffold, cells, and bioactive components that enable the repair and regeneration of damaged tissues or organs. The scaffold enables the spatial distribution of cells and growth factors, while the cells provide biological functions that are regulated through bioactive components.[1,2] A promising scaffold material has to be biocompatible, biodegradable, give adequate mechanical support, and allow for cell adherence. Hydrogels are an excellent material class suitable as scaffolds due to their ability to absorb a high water content, mimic the extracellular matrix (ECM), and provide an environment for cell adhesion, proliferation, and differentiation.[3] The biological properties are often provided by natural polymers (e.g., fibrin, collagen, gelatin, alginate, and hyaluronic acid) that are known for their impeccable cell compatibility and resemblance to the extracellular matrices.[4−8] On the other hand, synthetic polymers (e.g., polyester, polyethylene oxide, or poly(ethylene glycol) based hydrogels) possess high mechanical strengths and are highly reproducible.[9−11]

In recent years, interpenetrating polymer networks (IPNs), consisting of two or more combined polymers, have been used extensively as scaffolds in TE.[12−14] In comparison to conventional hydrogels composed of one polymer, IPNs can exhibit improved mechanical properties, increase in phase and thermal stability, and possess greater pore size with higher permeability.[12,15,16] In general, these IPNs are often composed of a natural hydrogel regulating the biological function and a second polymer contributing to the mechanical stiffness.[6,12,14−19]

Fibrin, a natural biopolymer, is commonly chosen as a biomaterial due to its many beneficial biological properties, such as remarkable cell adhesion, proliferation, and differentiation properties and the ability to build matrices that mimic the ECM. The natural abundance in human blood plasma and its role in wound healing, hemostasis, angiogenesis, and matrix interaction, leads to reduced risk of inflammation and rejection of autologous extractions from patients.[20,21] Fibrin is formed through the initiation by thrombin from the precursor fibrinogen. Fibrinogen has three types of polypeptides 2Aα, 2Bβ, and 2γ, which are connected through disulfide bridges. Thrombin removes the N-terminal fibrinopeptides of fibrinogen, exposing the α- and β- "knobs" to the a- and b- "holes", which leads to the assembly of the fibrin monomer to protofibrils. The formed fibrin can be degraded through

Received: March 15, 2023
Revised: June 2, 2023
Published: August 14, 2023

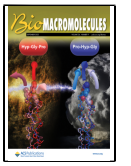

Table 1. Overview of Fibrin−Dextran Hydrogels[a]

hydrogel Fib_xD_y	m (fib.) [mg]	m (dextran-MA) [mg]	m (DTT) [mg]	% w/v (fib)	% w/v (dextran-MA)	n (DTT)/n (dextran-MA)
$Fib_{1.5}D_{2.5}$	2.97	5	0.5	1.5	2.5	0.2
$Fib_{1.5}D_5$	2.97	10	1	1.5	5.0	0.2
$Fib_{1.5}D_{7.5}$	2.97	15	1.5	1.5	7.5	0.2
$Fib_{1.5}D_{10}$	2.97	20	2	1.5	10.0	0.2
$Fib_{1.5}D_{10}$-a	2.97	20	1	1.5	10.0	0.1
$Fib_{1.5}D_{10}$-b	2.97	20	4	1.5	10.0	0.4
$Fib_{1.5}D_{10}$-c	2.97	20	20	1.5	10.0	1.0
$Fib_{0.7}D_{7.5}$	1.46	15	1.5	0.7	7.5	0.2
$Fib_{2.2}D_{7.5}$	4.46	15	1.5	2.2	7.5	0.2

[a]Fib, fibrin; D, dextran-MA; x = % w/v of fibrin; y = % w/v of dextran-MA.

fibrinolysis, where the enzyme plasmin breaks down the fibrin into fibrinopeptides and D-dimers.[22,23] In vivo, these two processes, formation and degradation of fibrin, lie in dynamic equilibrium and are regulated by the human body. Furthermore, the structural properties, e.g., fiber thickness, lengths, and porosity of fibrin are dependent on the pH, salt, and thrombin concentration.[22,24] In addition to the impeccable biological properties, fibrin hydrogels possess unique biomechanical and viscoelastic characteristics that lead to stiffening of the fibrin when exposed to high shear, tension, or compression, making them suitable to withstand deformations caused by the body.[25,26] A major disadvantage of pure fibrin hydrogels is their fast degradation, batch-to-batch variation, and low mechanical stiffness.[4] Approaches to overcome these challenges include the incorporation of additives, such as anti-fibrinolytic agents, e.g., tranexamic acid or synthetic polymers, e.g., polyethylene glycol, copolymer based on (hydroxyethyl)methacrylate and *N*-hydroxysuccinimide methacrylate or *N*-vinylpyrrolidone and glycidyl methacrylate.[17,27−29] The addition of these polymers have improved the mechanical stiffness and reduced the degradation rate.[28,29] However, the long-term effect of these synthetic polymers and their biodegradability are unknown. Therefore, an IPN based solely on bio-based materials, with the second component improving the mechanical stiffness, is desirable.

Dextran is a non-toxic, biodegradable, and water-soluble biopolymer, composed of α-1,6 D-glucopyranose with branching along α-1,2, α-1,3, and α-1,4 side chains.[30] These outstanding properties are the reason why dextran-based materials have been used in many applications, such as the food industry, pharmaceuticals, regenerative medicine, and TE. The natural production of dextran is accomplished by lactic acid bacteria, which can vary in molecular weight, linkages, and branches.[7,30] The biodegradation of dextran in mammals, e.g., human tissue, is controlled by dextranase.[31] In addition to the biodegradability, hydrophilicity, and biocompatibility of dextran, it is also cheap to produce and can easily be modified through reactions with hydroxyl groups.[7,32−34] Many investigations to incorporate new functional groups in dextran, e.g., carboxy-, methacrylate, or thiol groups have been introduced.[34−37] Zhang et al. used chloroacetate for the carboxymethylation of dextran, enabling a binding site to amines.[35] Thiolated-dextran was synthesized by Choi et al. by reacting dextran with mercaptopropionic acid.[37] To obtain terminal double bonds, van Dijk-Wolthuis et al. have reported the modification of dextran with glycidyl methacrylate (dextran-MA), which can then form dextran hydrogels through photo-initiation, or thiols via Michael addition.[34,38] By using dithiol, e.g., dithiothreitol (DTT), for crosslinking, injectable hydrogels can be obtained as these hydrogels can be formed in situ.[33] To the best of our knowledge, the combination of fibrin and dextran to fabricate hydrogels has not been reported so far.

In this work, we synthesized novel fibrin and dextran-MA-based hydrogels and determined their suitability as scaffolds for cell proliferation and differentiation. The mechanical properties of these new hydrogels were determined via rheology and compared to pure fibrin and dextran-MA hydrogels. Imaging methods, such as 2-photon microscopy and cryo-scanning electron microscopy (SEM), were utilized for visualizing fibrin−dextran hydrogels and to determine the fiber thickness. Based on these results and using ^{1}H NMR diffusometry, the mesh sizes were determined. Cell viability tests with L929 mouse fibroblasts and human mesenchymal stem cells (MSCs) were performed. Finally, degradation experiments of the fibrin−dextran hydrogels were conducted using a D-dimer enzyme-linked immunosorbent assay (ELISA).

2. MATERIALS AND METHODS

2.1. Materials. Dextran 150 kDA was purchased from VWR International. Glycidyl methacrylate was purchased from Sigma-Aldrich and distilled before use. Other chemicals purchased from Sigma-Aldrich include 4-dimethylaminopyridine, dimethyl sulfoxide, fibrinogen from human plasma (35−65% protein), and thrombin from human plasma (≥1000 NIH units mg^{-1} protein). DTT was purchased from Carbolution.

2.2. Methods. *2.2.1. Purification of Fibrinogen.* Five hundred mg of fibrinogen was diluted in 6.25 mL of $GBSH_5$-incomplete buffer (0.37 g L^{-1} KCl, 0.2 g L^{-1} $MgCl_2$ in 6·H_2O, 0.15 g L^{-1} $MgSO_4$ in 7·H_2O, 7.00 g L^{-1} NaCl, 0.12 g L^{-1} Na_2HPO_4, 1.19 g L^{-1} HEPES) and 6.25 mL of aqua ad injectable. The solution was dialyzed for 24 h at 4 °C against $GBSH_5$-incomplete buffer and stored at −80 °C until use.

2.2.2. Synthesis of Dextran-MA. The dextran-MA was synthesized according to the literature by van Dijk-Wolthuis et al.[34] First, glycidyl methacrylate was distilled to remove the hydroquinone stabilizer. Under an inert atmosphere, dextran (10.02 g, 0.062 mol, 1 equiv) was dissolved in dimethyl sulfoxide (70 mL). After dissolving the dextran, 4-dimethylaminopyridine (2.00 g, 0.016 mol, 0.3 equiv) was added. The reaction was initiated by adding glycidyl methacrylate (10 mL, 10.7 g, 0.075 mol, 1.2 equiv). The solution was stirred at room temperature (RT) for 48 h. For purification the solution was neutralized to pH = 7 and dialyzed for 5 days at 4 °C. The product was obtained through lyophilization and yielded a white powder.

2.2.3. Preparation of Fibrin−Dextran-MA Hydrogels. Synthesis of the fibrin−dextran hydrogel was performed by addition of fibrinogen (40 mg mL^{-1}), $CaCl_2$ (50 mM), $GBSH_5$-incomplete buffer, and dextran-MA (100, 200, 300, 400 mg mL^{-1}) in a reaction tube. In a second reaction tube thrombin (40 U mL^{-1}) and crosslinking agent DTT were mixed and added to the fibrinogen/dextran-MA mixture. The concentration of fibrinogen, $CaCl_2$, $GBSH_5$-buffer, and thrombin were chosen following an established protocol.[29] Thrombin was used to cleave fibrinogen, and $CaCl_2$ was chosen to accelerate the fibrin

https://doi.org/10.1021/acs.biomac.3c00269
Biomacromolecules 2023, 24, 3972−3984

polymerization.[22,39] The hydrogel was placed in an incubator for 1 h at 37 °C to ensure complete gelation. The compositions of fibrin and dextran are listed in Table 1 with variation in dextran amount ($Fib_{1.5}D_{2.5}$–$Fib_{1.5}D_{10}$), DTT amount ($Fib_{1.5}D_{10}$-a–$Fib_{1.5}D_{10}$-c) and fibrinogen amount ($Fib_{0.7}D_{7.5}$–$Fib_{2.2}D_{7.5}$).

2.2.4. Rheological Characterization of Fibrin–Dextran-MA Hydrogels. The rheological characterization was conducted on a TA Instrument Discovery HR-3 hybrid rheometer using a 20 mm cone-plate geometry with a cone angle of 2° at 37 °C. The hydrogels were prepared as described in Section 2.2.3. The gelation properties of the hydrogel were determined using time-dependent measurements for 45 min at a frequency of 1 Hz and 0.1% strain. Afterwards, frequency-dependent measurement was proceeded with varying frequencies from 0.01 to 10 Hz at a constant strain of 1%. Finally, oscillation-dependent measurement was performed with varying strains between 0.1 and 1000% at 0.1 Hz to investigate the strain-stiffening/softening properties.

2.2.5. Nanoindentation of Fibrin–Dextran-MA Hydrogels. The nanoindentation was conducted at RT on a Pavone nanoindenter by Optics Life. All measurements were performed with a cantilever with a stiffness k of 0.21 N m^{-1} and a tip radius of 29.5 μm. Two of each hydrogel were prepared in a 24-well plate as described in Section 2.2.3 and measured on the same day. Each sample was indented three times at four to eight different points on the surface of the hydrogels.

2.2.6. Swelling Experiments of Fibrin–Dextran-MA Hydrogels. The samples were prepared as described in Section 2.2.3 and immersed in buffer overnight. The weight of the swollen gels was recorded as (w) and dried by using a vacuum oven at 60 °C or freeze-dried. The dry weight (w_0) was noted after 72 h, and the swelling ratio $\langle Q \rangle$ was calculated with eq 1.

$$Q = \frac{w - w_0}{w_0} \times 100 \tag{1}$$

2.2.7. Degradation Studies. Gravimetrical analysis of the degradation of the hydrogels was conducted for 20 days. The hydrogels were prepared as described in Section 2.2.3 in a vial and the initial weight determined. After incubating the hydrogels for 1 h at 37 °C to ensure full gelation, the hydrogels were placed in buffer solution. The hydrogels were allowed to swell for 24 h. The buffer solution was removed and the weights were taken every 24 h until full degradation of the hydrogel or 20 days have passed. After the notation of the weights, fresh buffer solution was added.

2.2.8. Cryo-SEM of Fibrin–Dextran-MA Hydrogels. The cryo-SEM images of the hydrogels were taken on a cold field emission SEM (FE-SEM/S4800) equipped with a Gatan cryo-Chamber. The hydrogel samples were prepared as described in Section 2.2.3. For analysis, the samples were frozen with liquid nitrogen, placed in a sample holder and transferred into a preparation chamber under vacuum. The upper layer of the sample was broken off by razor blade, while under cooling with liquid nitrogen inside the preparation chamber. The samples were measured at 2 μA with 1.0 kV with an SE detector.

2.2.9. NMR Diffusometry of Fibrin–Dextran-MA Hydrogels. The effective diffusivity D of water absorbed at saturation in fibrin–dextran-MA hydrogels was measured using a low-field, time-domain Bruker minispec mq20 NMR spectrometer working at 20 MHz. The pulsed-field-gradient stimulated echo (PFGSE) sequence of Stejskal–Tanner was used and the temperature was stabilized at 23 °C.[40] In these experiments, only the ^{1}H NMR signal of free water molecules with high mobility is detected due to the longer lifetime of stimulated spin-echo. The bound water to polymer chains and polymer network stimulated spin echoes are filtered out by the time-domain parameters used in these experiments.

The NMR diffusometry experiment used in this study is one-dimensional, by recording the dependence of the spin-echo integral intensity upon the applied field gradient strength. The apparent diffusivity was obtained by fitting the normalized stimulated spin-echo decay as a function of gradient strength g, given by Stejskal–Tanner eq 2, where we employ the convention $q = \gamma\delta g$, for the diffusion wave vector and magnetogyric ratio γ in units of rad s^{-1} T^{-1}.[40−43]

$$\frac{E(g)}{E_0} = \exp\left\{-q^2 D\left(\Delta - \frac{\delta}{3}\right)\right\} \tag{2}$$

In the equation above, $E(g)$ is the integral intensity of the stimulated spin echo at a given value of the magnetic field gradient g, and E_0 is the integral intensity for a small value of the field gradient compared to the maximum of the gradient strength. The duration of the gradient pulse is denoted by δ, while Δ is the diffusion time defined as the time interval between the gradient pulses. In all the ^{1}H NMR diffusometry experiments reported in this study, the delays were set to δ = 1 ms, Δ = 10 ms, and a relaxation delay of 5 s was used. The stimulated spin-echo was detected with a receiver window of 0.5 ms. The field gradient g was applied in the z direction and incremented in 40 steps with a linear ramp from 1 to 90% of the maximum field gradient g_{max} = 3.57 T m^{-1}.

2.2.10. Two-Photon Laser Scanning Microscopy of Fibrin–Dextran-MA Hydrogels. To visualize the fibrin part of the hydrogel, fibrinogen was stained with Alexa Fluor-488 before the hydrogel preparation. The hydrogels were prepared according to the description in Section 2.2.3. Instead of fibrinogen (40 mg mL^{-1}), stained fibrinogen with Alexa Fluor-488 was used and the samples were washed three times with buffer. A Leica stellaris 8 dive falcon was used for image acquisition equipped with a spectra physics insight X3 dual laser and 4Tune HYD RLD detector and HC IRAPO L 25x/1.00 W motCORR objective. The samples were measured at an excitation wavelength of 800 nm and a detection band between 482 and 534 nm.

2.2.11. Cell Culture. All cell culture experiments were approved by the local ethics committee from RWTH Aachen University (EK 300/13) and carried out under a laminar flow workbench. All surface tops and materials were disinfected with 70% ethanol prior to their use in the workbench; the latter was additionally treated with UV light afterward. Cell culture media and phosphate-buffered saline (PBS; Gibco, Darmstadt, Germany) were preheated in a water bath (approximately 37 °C) before usage. Cells were cultured in a 20% O_2 and 5% CO_2 humidified atmosphere at 37 °C. All cells were tested for possible mycoplasma contaminations before the experiments were performed.

2.2.12. Human Mesenchymal Stem Cells. Human mesenchymal stromal or stem cells (MSCs) used in this work were derived from the bone marrow of explanted femoral heads, anonymously provided by the Orthopedic Clinic of RWTH Aachen University Hospital. Cells were isolated according to protocols from Pittenger et al. and Haynesworth et al. as previously described.[29,44,45] Femoral heads were surgically removed from patients undergoing total hip endoprosthesis (TEP) and obtained following informed consent. First, the bone marrow spongiosa was repeatedly rinsed with fresh stem cell medium (SCM, Mesenpan, PanBiotech, Aidenbach, Germany) containing 25 mg plasmocin (InvivoGen, Toulouse, France). Mesenpan SCM contains 1% ITS-plus (insulin–transferrin–selenic acid and bovine serum albumin (BSA)–linoleic acid, Pan-Biotech, Aidenbach, Germany), 1 nm dexamethasone (Pan-Biotech, Aidenbach, Germany), 100 μm ascorbic acid-2-phosphate (Pan-Biotech, Aidenbach, Germany), 10 ng mL^{-1} epidermal growth factor (EGF, Pan-Biotech, Aidenbach, Germany), 1% penicillin (80 U mL^{-1}, Gibco, Darmstadt, Germany), 1% streptomycin (80 μg mL^{-1}, Gibco, Darmstadt, Germany), and 1% L-glutamine (1.6 mM, Gibco, Darmstadt, Germany). Penicillin, streptomycin, L-glutamine, 2% of fetal calf serum (FCS, Pan-Biotech, Aidenbach, Germany), and 25 mg plasmocin were added.

Second, the medium containing MSC solution was centrifuged for 10 min at 500g. Next, the supernatant was aspirated, the cell pellet resuspended in 10 mL of PBS and centrifuged for 10 min at 500g. Thereafter, the supernatant was aspirated again, the remaining cell sediment were resuspended in SCM, cells were seeded in a T75 cell culture flask (Cellstar, Greiner bio-one, Frickenhausen, Germany), and subsequently placed in an incubator. After 24 h of incubation, the medium was removed and cells were rinsed with 10 mL of PBS to remove remaining non-adherent (hematopoietic) cells, bone fragments, and erythrocytes. Afterward, 10 mL of fresh SCM was added

https://doi.org/10.1021/acs.biomac.3c00269
Biomacromolecules 2023, 24, 3972−3984

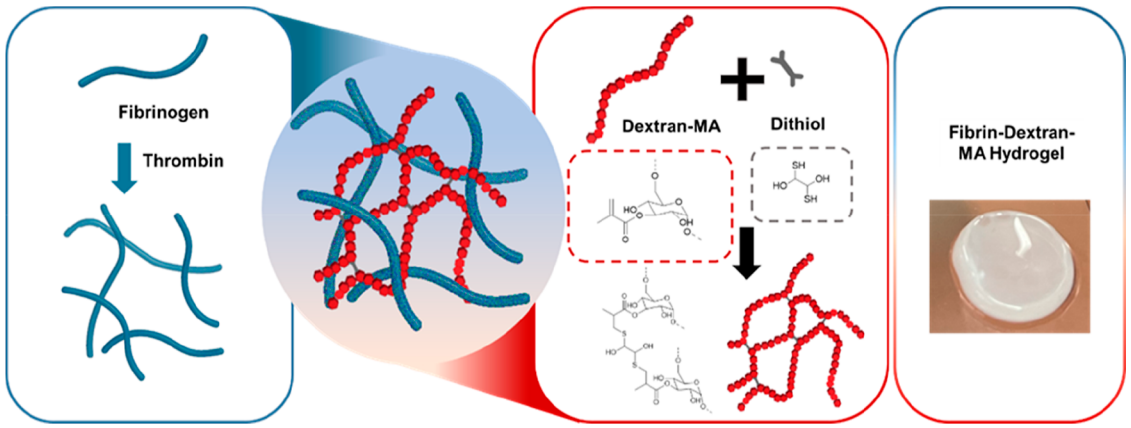

Figure 1. Schematic representation of fibrin−dextran interpenetrating hydrogel networks.

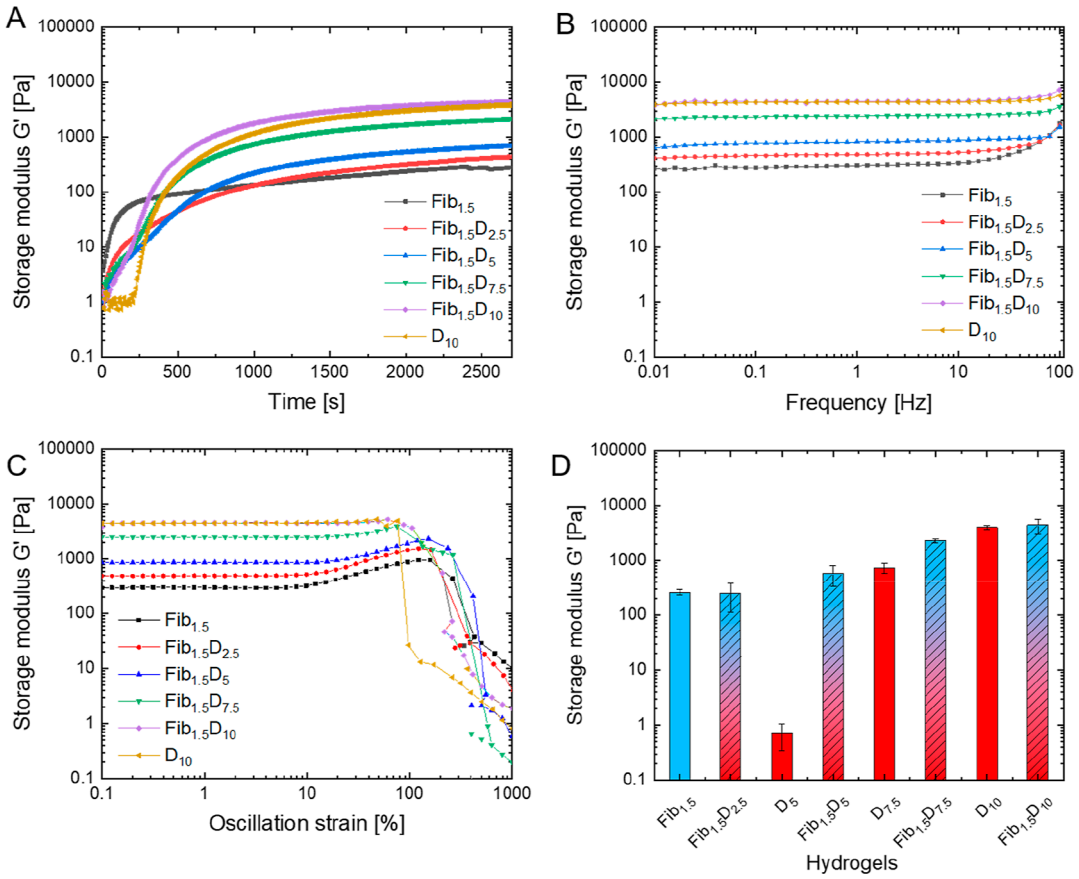

Figure 2. Rheological measurements of pure fibrin, dextran hydrogels, and fibrin−dextran hydrogels with (A) gelation time, (B) frequency-dependent measurement and (C) oscillation-dependent measurement. Figure (D) shows an overview of the storage modulus for all hydrogels.

and the medium was changed twice per week. Once the cells reached a confluence of 80−90%, they were trypsinized with 4 mL of 0.01% trypsin (Lonza, Cologne, Germany) and reseeded in fresh SCM at a density of 5 × 10^3 cells cm^{-2} for optimum proliferation. Flow cytometry for surface epitope characterization and multipotency was demonstrated to characterize stem cells using standard protocols as previously described.[46]

2.2.13. L929 Mouse Fibroblast Cell Line. Mouse fibroblasts of the L929 cell line (ATCC, Wesel, Germany) were also used to evaluate the cytotoxicity of dextran-MA in combination with fibrin according to ISO 10993-5. Cells were cultured in Roswell Park Memorial Institute (RPMI) 1640 medium (Gibco, Darmstadt, Germany) and supplemented with 5% newborn calf serum (NCS, Gibco, Darmstadt, Germany), 1% penicillin (80 U mL^{-1}, Gibco, Darmstadt, Germany), 1% streptomycin (80 μg mL^{-1}, Gibco, Darmstadt, Germany), and 1% L-glutamine (1.6 mM, Gibco, Darmstadt, Germany). The medium was changed twice a week and cells were harvested at approximately 90% confluency and trypsinized with 6 mL of 0.25% trypsin (Lonza, Cologne, Germany).

2.2.14. Cytotoxicity/Viability Test According to ISO 10993-5. To detect cytocompatibility/cytotoxicity of dextran in combination with fibrin, live/dead staining of human stem cells and mouse fibroblasts on biomaterials was performed after 1, 3, and 7 days of seeding according to protocols 10993−5 of the International Standardization Organization (ISO). Briefly, 600 μL of Ringer solution (B. Braun, Melsungen, Germany) was mixed with 10 μL of fluorescein diacetate (FDA, 5 mg mL^{-1} in acetone, Sigma-Aldrich, Steinheim, Germany), and 10 μL of propidium iodide (PI, 0.5 mg mL^{-1} in PBS, Sigma-

https://doi.org/10.1021/acs.biomac.3c00269
Biomacromolecules 2023, 24, 3972−3984

Aldrich, Steinheim, Germany). Cells were stained with 20 μL of this stock solution and analyzed using fluorescence microscopy (DMI6000B, Leica, Wetzlar, Germany). The double staining with FDA/PI allows us to differentiate between viable and dead cells. Viable cells emit a green fluorescence, whereas a red fluorescence indicates dead cells. For the dead cell controls, 20 μL of TritonX-100 (0.1% dissolved in PBS, Sigma-Aldrich, Steinheim, Germany) was added to lyze the cells. Initial cell seeding density was dependent on the cell type due to different cell sizes: 5×10^3 cells cm^{-2} for MSC and 1.8×10^4 cells cm^{-2} for L929 mouse fibroblasts.

2.2.15. D-Dimer Human ELISA. To determine the rate of fibrinolysis and whether the used dextran influences the degradation process, the human D-dimer ELISA (Thermo Fisher Scientific, Dreieich, Germany) was performed according to the manufacturer's instructions.

The test setup was carried out with different dextran concentrations (1, 2.5, or 5 mg mL^{-1}) with MSCs. Human MSCs were seeded in a density of 5×10^3 cells cm^{-2}. Medium was collected from the samples after 1 and 3 days and stored at −80 °C. Hydrogel samples were prepared as triplicates and the standard curve conducted as duplicates. Supernatant was removed after cultivation and was diluted 1:5 with the provided assay diluent.

3. RESULTS AND DISCUSSION

3.1. Hydrogel Fabrication. Dextran-MA is synthesized based on the procedure described by van Dijk-Wolthuis, by coupling glycidyl methacrylate to dextran (Mw = 150 kDA) in dimethylsulfoxide.[34] The characterization of dextran-MA can be found in the Supporting Information Figures S1 and S2. The fibrin- and dextran-based hydrogels are formed through simultaneous in situ gelation of the fibrin hydrogel and dextran-MA hydrogel. For the fibrin hydrogel part, thrombin is mixed with soluble fibrinogen, leading to cleavage of fibrinopeptides and the formation of insoluble fibrin as described by Weisel et al.[22] Simultaneously, the methacrylate groups of dextran-MA are able to react with the thiol groups of DTT via Michael addition to form a hydrogel.[47] As both, fibrin and dextran-MA hydrogel systems undergo crosslinking by different mechanisms, we propose that the formed network topology is similar to IPNs (Figure 1). The fibrin−dextran-based hydrogels are obtained within a few minutes and the gelation is confirmed through the tilting method and rheology.

3.2. Gelation Time. To determine the gelation time of the hydrogels, rheology measurements were conducted (Figure 2). The gelation time of the hydrogels is listed in Table 2. The reference sample of the fibrin hydrogel undergoes gelation instantaneously, as shown through the rapid increase in storage modulus G' in Figure 2A. This is in accordance with the results obtained by Wedgwood et al., who observed gelation of fibrin hydrogels within a few minutes.[48] In contrast, the gelation time of the reference sample of the dextran-MA hydrogel with the highest dextran concentration of 10 w/v % starts at 212 ± 5 s (3−4 min), which is in the range of values acquired by Liu et al.[33] Both, fibrin and dextran-MA reference samples, only exhibit one gelation point, while the fibrin−dextran hydrogels show two independent gelation points. The first increase in storage modulus of all hydrogel blends occurs instantaneously, which is attributed to the gelation of fibrin hydrogels triggered by thrombin. A second increase in the storage modulus can be seen for all hydrogel blends, which is a result of the gelation of the dextran hydrogel part. The change in gelation behavior for two component systems was also observed by the group of Rahimi-Movaghar et al. for fibrin combined with Wharton's-jelly-extract.[49] A correlation between high amounts of dextran-MA and increased gelation is observed, where the fastest gelation was obtained for $Fib_{1.5}D_{10}$. Furthermore, the second gelation point occurs faster for all hydrogel blends than the corresponding pure dextran hydrogels with the same dextran-MA concentration. A reason for this can be that the methacrylate groups of dextran or dithiol interact with thiol groups of fibrinogen via Michael addition or disulfide bridging, leading to the acceleration of the gelation process. Contrary to this observation, the investigation of Blomback et al. showed a slower degradation of fibrin hydrogels through the addition of dithiol due to the reduction of disulfide bonds in the absence of calcium ions and a negligible influence in the presence of calcium ions.[50] However, factor XIII was used in the study by Blomback et al. and the influence of dextran-MA was not tested. In addition, the results of our studies showed that the cross-linker dithiol influences the gelation process. Another possible explanation could be that the calcium ions affect the gelation of dextran-MA. The fastest gelation is observed for the lowest amount of dithiol cross-linker ($Fib_{1.5}D_{2.5}$−$DTT_{0.1}$) at 169 ± 5 s and the slowest gelation is observed with the highest amount of dithiol ($Fib_{1.5}D_{2.5}$−$DTT_{1.0}$) at 382 ± 5 s. This leads to the assumption that high amounts of dithiol inhibit the gelation process due to saturation of the dextran-MA binding sites, i.e., the double bonds. A reason for this could be that for successful gelation of the hydrogel via crosslinking, both thiol groups of one DTT molecule need to react with two different dextran-MA strands. At high dithiol concentrations, the ratio between present thiol groups and dextran binding sites will lead predominantly to the reaction of one thiol group of DTT with methacrylate groups of dextran and therefore, no crosslinking can occur.

Table 2. Overview of the Hydrogel's Gelation Times

hydrogel	n (DTT)/n (dextran-MA) [mol/mol]	gelation time 1 [s]	gelation time 2 [s]
$Fib_{1.5}$		instant	
$D_{2.5}$	0.2	no gelation	
D_5	0.2	504 ± 5	
$D_{7.5}$	0.2	334 ± 5	
D_{10}	0.2	212 ± 5	
$Fib_{1.5}D_{2.5}$	0.2	instant	309 ± 10
$Fib_{1.5}D_5$	0.2	instant	267 ± 10
$Fib_{1.5}D_{7.5}$	0.2	instant	218 ± 10
$Fib_{1.5}D_{10}$	0.2	instant	200 ± 10
$Fib_{1.5}D_{10}$-a	0.1	instant	169 ± 10
$Fib_{1.5}D_{10}$-b	0.4	instant	182 ± 10
$Fib_{1.5}D_{10}$-c	1.0	instant	382 ± 10

3.3. Mechanical Properties of Fibrin−Dextran-MA Hydrogels. Rheological tests were conducted to assess the mechanical properties of the obtained hydrogels (Figures 2 and S7). An overview of the average storage moduli of all hydrogels is listed in Table 3. All hydrogels exhibit higher storage modulus compared to the reference sample of pure fibrin. A clear correlation between dextran-MA concentration and storage modulus G' can be detected, with the highest storage modulus achieved for $Fib_{1.5}D_{10}$ at 4765 ± 1280 Pa. In addition, a significantly slower gelation time can be observed for the fibrin−dextran hydrogels with low amounts of dextran-MA compared to pure dextran hydrogels. This can be observed, for example, for $Fib_{1.5}D_{2.5}$, which gelates instantly and has a storage modulus of 244 ± 132 Pa, while no gelation occurs for the reference dextran hydrogel sample $D_{2.5}$. A reason for this is that the gelation of $Fib_{1.5}D_{2.5}$ is dominated by

https://doi.org/10.1021/acs.biomac.3c00269
Biomacromolecules 2023, 24, 3972−3984

Table 3. Overview of Average Storage Moduli G' of Hydrogels[a]

hydrogel	mass (fibrin) [mg]	mass (dextran-MA) [mg]	mass (DTT) [mg]	storage modulus G' [Pa]	loss modulus G'' [Pa]
$Fib_{1.5}$	2.97	0	0	259 ± 30	15 ± 14
$D_{2.5}$	0	5	0.5	no gelation	no gelation
D_5	0	10	1	0.7 ± 0.4	0.07 ± 0.05
$D_{7.5}$	0	15	1.5	746 ± 155	0.79 ± 0.19
D_{10}	0	20	2	4006 ± 342	16 ± 15
$Fib_{1.5}D_{2.5}$	2.97	5	0.5	244 ± 132	10 ± 4
$Fib_{1.5}D_5$	2.97	10	1	566 ± 238	18 ± 6
$Fib_{1.5}D_{7.5}$	2.97	15	1.5	2281 ± 184	30 ± 6
$Fib_{1.5}D_{10}$	2.97	20	2	4765 ± 1280	25 ± 5
$Fib_{1.5}D_{10}$-a	2.97	20	1	1640 ± 182	14 ± 2
$Fib_{1.5}D_{10}$-b	2.97	20	4	4836 ± 126	22 ± 7
$Fib_{1.5}D_{10}$-c	2.97	20	20	1970 ± 1411	9 ± 6

[a] p^* <0.001; p^* listed in Table S3.

fibrinogen, which exhibits a similar storage modulus of 259 ± 30 Pa. For $Fib_{1.5}D_5$, a significantly higher storage modulus of 746 ± 155 Pa is obtained in comparison to dextran hydrogel D_5 at 0.7 ± 0.4 Pa and the fibrin hydrogel at 259 ± 30 Pa. This could be a result of a synergetic effect caused by interpenetrating networks of the fibrin and dextran hydrogels. This effect is less significant for $Fib_{1.5}D_{7.5}$ and $Fib_{1.5}D_{10}$, as the differences in storage modulus decrease for $D_{7.5}$ and D_{10}. Here, it seems that for higher dextran-MA amounts, the dextran hydrogel part dominates. For the frequency-dependent measurements, all hydrogels exhibit a frequency-independent behavior up until at least 10 Hz (Figure 2B), which confirms the formation of a hydrogel.

The measurements based on the oscillation-dependency show strain-stiffening behavior for the pure fibrin hydrogel, $Fib_{1.5}D_{2.5}$, and $Fib_{1.5}D_5$, which can be detected by the increase in storage modulus above 10% strain (Figure 2C). This strain-stiffening behavior is caused by the elastic properties of fiber-like fibrin networks and has previously been reported.[2,48,51] For $Fib_{1.5}D_{7.5}$, a minimal strain-stiffening behavior occurs. In comparison, the pure dextran-MA hydrogel and $Fib_{1.5}D_{10}$ exhibit strain-softening behavior, which can be seen through the decrease of the storage modulus at 48 and 61% strain. For the dextran-MA hydrogel, this decrease arises rapidly at 48% strain, which is below all fibrin−dextran hydrogels and the pure fibrin hydrogel.

As $Fib_{1.5}D_5$, $Fib_{1.5}D_{7.5}$, and $Fib_{1.5}D_{10}$ show the most promising mechanical properties, these were investigated in the following sections.

3.4. Nanoindentation. The fibrin−dextran-MA hydrogels were analyzed via nanoindentation (Figure 3). The reference sample of the pure fibrin hydrogel has the lowest Youngs' modulus with 1.0 ± 0.3 Pa and pure dextran hydrogels has a stiffness of 7.5 ± 2.5 kPa. All fibrin−dextran-MA hydrogels exhibit higher Youngs' moduli than the pure fibrin hydrogel with $Fib_{1.5}D_5$ (3.2 ± 0.7 kPa) to $Fib_{1.5}D_{7.5}$ (8.6 ± 2.3 kPa) and $Fib_{1.5}D_{10}$ (28.8 ± 20.3 kPa). A correlation between increasing dextran-MA and higher Youngs' modulus can be seen, which is in accordance with the results obtained from rheology. Overall, there is a large scattering of the indentation values, which could be due to the random distribution of the different fiber types in the interpenetrating hydrogel network. In addition, only a small area (tip radius = 29.5 μm) is indented, which means that the values could vary depending on the position where the measurement is performed.

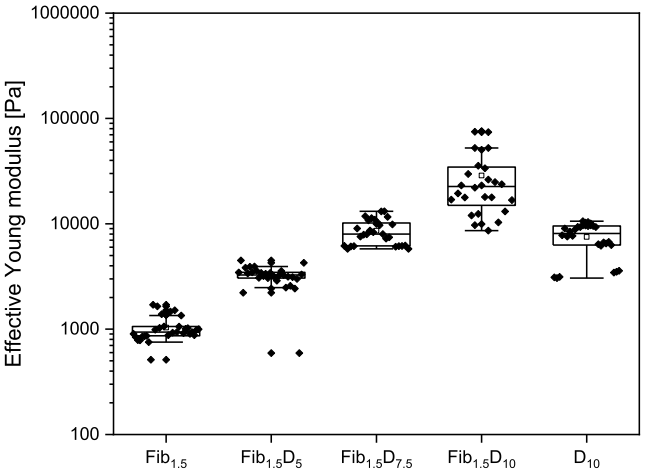

Figure 3. Effective Youngs' modulus of the fibrin hydrogel($Fib_{1.5}$), fibrin−dextran-MA hydrogels ($Fib_{1.5}D_{5-10}$), and the dextran-MA hydrogel (D_{10}).

3.5. Structure and Mesh Size of Fibrin−Dextran-MA Hydrogels. The pore sizes of fibrin−dextran-MA hydrogels are related to the mesh sizes, which are important parameters for establishing the correlation of stiffness/permeability and designing scaffolds.[52−54] To gain information about the structures of fibrin−dextran-MA hydrogels, cryo-SEM was used (Figure 4). These images showed that the pure fibrin hydrogel forms thin, branched fibers with a web-like structure, which has been reported in the literature.[2] In comparison, the pure dextran-MA hydrogel forms dense pore structures with small uniform pores. According to Liu et al., these small and homogenous pores can be explained by the high functionalization degree of dextran-MA that enabled high crosslinking with dithiol.[33] All fibrin−dextran-MA hydrogels show a combined structure of elongated fibers, which typically occur in fibrin and predefined pore structures, typical for dextran-MA hydrogels. Furthermore, it can be observed that with increasing dextran-MA concentration, the dextran-MA structure dominates, building a more rigid structure. Regarding the pore structure, it is evident that the fibrin hydrogel possesses large pores (Figure 4A) compared to the dextran-MA hydrogel (Figure 4B). The pore sizes of fibrin are not uniformly distributed in space and are several times bigger on average compared to those of the dextran-MA hydrogel. From Figure 4, it can be observed that the pore size of high dextran-MA concentration ($Fib_{1.5}D_{10}$) is smaller than the pore sizes of $Fib_{1.5}D_5$ and

https://doi.org/10.1021/acs.biomac.3c00269
Biomacromolecules 2023, 24, 3972−3984

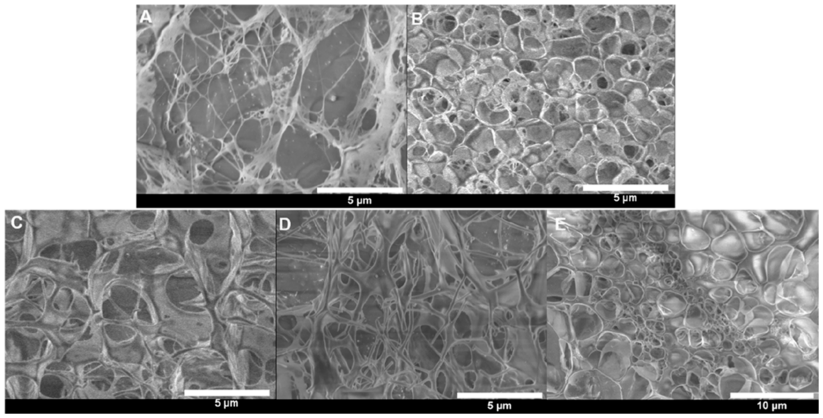

Figure 4. Overview of cryo-SEM microscopy images of (A) a pure fibrin hydrogel, (B) a pure dextran hydrogel D_{10}, (C) $Fib_{1.5}D_5$, (D) $Fib_{1.5}D_{7.5}$, and (E) $Fib_{1.5}D_{10}$ with a scale bar of 5 μm.

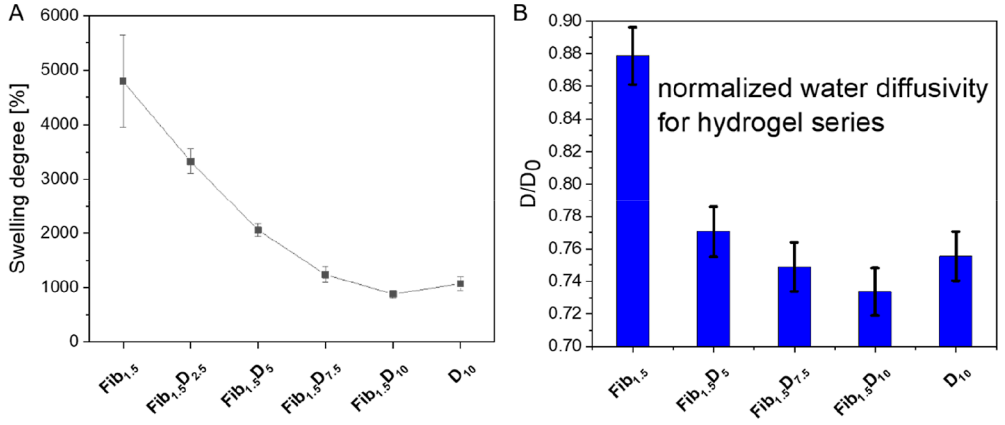

Figure 5. (A) Swelling degree and (B) water diffusivity of pure fibrin, the pure dextran-MA hydrogel, $Fib_{1.5}D_5$, $Fib_{1.5}D_{7.5}$, and $Fib_{1.5}D_{10}$.

$Fib_{1.5}D_{7.5}$. This could be a result of the higher crosslinking due to increased dextran-MA content leading to smaller pores.[33] In general, the pore sizes for fabricated hydrogels are situated between that of fibrin and dextran-MA hydrogels.

In order to estimate the mesh size ξ, the hydrated radius (r_f) of the polymer chain and water diffusion coefficient have to be measured (eq 3). Cryo-SEM pictures presented in Figure 4 can be employed to obtain an average value of r_f using ImageJ software. For the fibrin hydrogel, the average fiber thickness ($d_f = 2r_f$) is presented in Figure S3 and has the value $2r_f \approx 150 \pm 44$ nm. This value is in agreement with those reported by Ryan et al. and Ferri et al., for fibrin hydrogels using SEM and elastic light scattering techniques.[55,56] The dextran-MA fibers have a smaller radius compared to the fibrin fibers. Therefore, the evaluation of r_f from Figure 4B is affected by larger errors. Hence, in the following we use the mean apparent radius of dextran from size-exclusion chromatography reported by Williams et al., i.e., $r_f \approx 64$ nm.[57] This value is close to the mode value of dextran-MA fibers with $r_f = 60$ nm obtained from Figure 4B.

The mesh size of hydrogels can be measured non-invasively and accurately by NMR diffusometry using the diffusivity of the solvent in the hydrogel. Recently, it was proven that obstruction models provide a good agreement with the correlation length of polymer networks and can be used to estimate the mesh size ξ, using the following relation (eq 3). Here, D is the water diffusion coefficient in the hydrogel and D_0 is the diffusivity of free water.[58,59]

$$\frac{D}{D_0} = \exp\left\{-\pi\left[\frac{r_s + r_f}{\xi + 2r_f}\right]^2\right\} \tag{3}$$

The solvent radius, i.e., water, is denoted by r_s ($r_{H_2O} = 0.15$ nm), and r_f is the hydrated radius of the polymer chain estimated above. From eq 3, the mesh size can be derived by

$$\xi = (r_s + r_f)\left\{\frac{1}{\pi}\ln\left[\frac{D_0}{D}\right]\right\}^{1/2} - 2r_f \tag{4}$$

The normalized diffusivity ratio D/D_0 of water has to be measured by NMR diffusometry. The dependences of the natural logarithm of stimulated echo $E(g)/E(0)$ as a function of q^2 are shown in Figure S4 for fibrin and dextran-MA hydrogels and for the fibrin−dextran-MA series. The effective diffusivity was obtained by fitting the normalized stimulated spin-echo decay as a function of q^2, using the Stejskal−Tanner equation as described in the experimental section.[40] From the water diffusivity data shown in Figure S4, we obtained the normalized effective diffusivity D/D_0 given in Figure 5 for all hydrogels. We can conclude that due to increased water diffusivity in the fibrin hydrogel compared to that of dextran, the pore sizes are larger in the former case. Furthermore, the pore sizes will decrease for hydrogels with an increasing dextran network component as reflected in the D/D_0 ratios.

The mesh sizes of the reference polymer networks can be evaluated from the data shown in Figure 5 and eq 4 and are

https://doi.org/10.1021/acs.biomac.3c00269
Biomacromolecules 2023, 24, 3972−3984

presented in Table 4. The trend in mesh size determined by diffusometry is in agreement with the findings of cryo-SEM, shown in Figure 4.

Table 4. Mesh Size ξ and Mesh Radius r_m, for Fibrin ($Fib_{1.5}$) and Dextran-MA (D_{10}) Hydrogels from Obstruction Modeleq 4 and Figure 5B and Effective Mesh Size $\langle\xi\rangle$ as Well as the Effective Mesh Radius $\langle r_m\rangle$, for IPN Hydrogels Using Equation: $\langle\xi\rangle = c_{Fib}\xi_{Fib} + c_D\xi_D$, Where$c_{Fib}$ and c_D are the Relative Content of Fibrin and Dextran Networks (Table S2)

hydrogels	mesh size $\xi/\langle\xi\rangle$ [nm][a]	mesh radius $r_m/\langle r_m\rangle$ [nm][a]
$Fib_{1.5}$	220	179.5
$Fib_{1.5}D_5$	116.9	95.4
$Fib_{1.5}D_{7.5}$	115.7	94.4
$Fib_{1.5}D_{10}$	103.6	84.5
D_{10}	86.4	70.5

[a]Errors are of the order of 10%.

Accordingly, to obtain the effective mesh size $\langle\xi\rangle$ of fibrin−dextran hydrogels, the relative content of fibrin and dextran used in the hydrogel formulations were taken into account, which are given in Table S2. As expected, the effective mesh size will decrease with an increase in the dextran content. This correlation is difficult to estimate from the cryo-SEM pictures in Figure 4. The smallest mesh size is obtained for the pure dextran-MA hydrogel with a value of 86.4 nm, which is slightly higher than the pore size reported by Liu et al.[33]

The hydrogel model structure used for the derivation of the results above implies that the network junctions are tetra-functional, i.e., $f = 4$, and all chains are restricted to a 2D plane. Besides, three-dimensional (3D) modeling of swollen polymer networks can provide a more realistic representation of the hydrogel space geometry.[60] The 3D lattice structures were used to introduce mesh radius r_m, which depend on both mesh size ξ, and junction functionality of the hydrogel network. For a tetra-functional network, the more realistic mesh radius is given by $r_m = \frac{\sqrt{6}}{3}\xi$. The corresponding effective mesh radius in case of hydrogel interpenetrating networks is given by $\langle r_m\rangle = \frac{\sqrt{6}}{3}\langle\xi\rangle$, where the quantities ξ and $\langle\xi\rangle$ are reported in Table 4.[60]

3.6. Swelling Degree of Fibrin−Dextran-MA Hydrogels. The swelling degree of the hydrogels was studied by incubating the hydrogels in buffer (pH = 8.4) overnight. The swelling degree of the hydrogels $Fib_{1.5}D_{2.5}$, $Fib_{1.5}D_5$, $Fib_{1.5}D_{7.5}$, $Fib_{1.5}D_{10}$, $Fib_{1.5}$ and D_{10} are shown in Figure 5. The fibrin hydrogel exhibits the highest swelling degree with 4793 ± 849%, which correlates well with the results obtained from NMR diffusivity and SEM images. These showed large pore sizes that are able to absorb high amounts of water. The swelling degree decreases with increasing dextran-MA concentration as higher dextran-MA concentrations form denser pore structures preventing the hydrogels to absorb water and swell, as it can be seen in the SEM images (Figure 4) and water diffusometry measurements (Figure 5B). The highest swelling degree for fibrin−dextran-MA hydrogels is achieved for $Fib_{1.5}D_{2.5}$ with 3330 ± 223%, followed by $Fib_{1.5}D_5$ with 2057 ± 116%, $Fib_{1.5}D_{7.5}$ with 1241 ± 145%, and the lowest swelling degree for $Fib_{1.5}D_{10}$ with 883 ± 72%. In comparison, the dextran-MA hydrogel has a low swelling degree with 1074 ± 122% due to the high crosslinking density, however, it is slightly higher than $Fib_{1.5}D_{10}$. A reason for this could be that the fibrin forms additional crosslinking through fibrinogen and thrombin in the hydrogel network. This leads to stiffer gels, as shown by the rheology measurements in Section 3.3, and thus leads to a lower ability to absorb water.[61,62]

3.7. Degradation of Fibrin−Dextran-MA Hydrogels. The degradation of pure fibrin, $Fib_{1.5}D_5$, $Fib_{1.5}D_{7.5}$, $Fib_{1.5}D_{10}$, and the pure dextran hydrogel (D_{10}) was conducted using gravimetric analysis after initial swelling for 24 h. The degradation of the hydrogels was monitored every 24 h for 20 days (480 h). The mass loss was determined using eq 5, where the weight at a specific time point (w_t) is divided by the swollen weight determined after 24 h (w).

$$\text{mass loss [\%]} = \left(\frac{w_t}{w}\right) \times 100 \tag{5}$$

Figure 6 shows the degradation profile of the hydrogels. The fastest degradation can be observed for the pure fibrin hydrogel

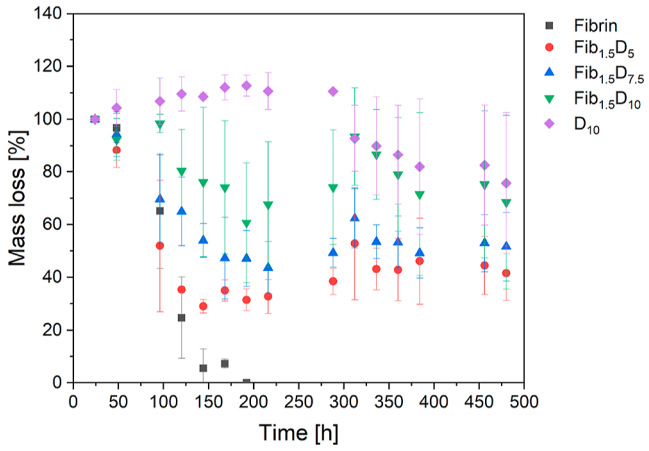

Figure 6. Degradation of hydrogels represented as time-dependent mass loss.

($Fib_{1.5}$), which fully degrades after 8 days (192 h). For fibrin−dextran-MA hydrogels, a slower degradation can be seen with increasing dextran-MA concentration. Thus, the fastest degradation of the fibrin−dextran-MA hydrogels was detected for $Fib_{1.5}D_5$, with a final mass of 30−40% after 6 days (144 h). $Fib_{1.5}D_{7.5}$ with medium dextran-MA amount, reaches a plateau of 40−50% after 6 days (144 h). The slowest degradation of the blends was observed for $Fib_{1.5}D_{10}$ with a mass 65−75% after 8 days (192 h). The dextran hydrogel (D_{10}) shows a slight increase of the mass within the first 12 days (288 h), which can be explained by additional water uptake. After 13 days (312 h), the dextran hydrogel (D_{10}) begins to degrade and reaches a final mass of 75% after 20 days. To conclude, the results show that the addition of dextran-MA to form fibrin−dextran-MA hydrogels lead to slower degradation rates compared to the pure fibrin hydrogel.

3.8. Visualization of Fibrin Structure in Fibrin−Dextran-MA Hydrogels. To visualize the selected hydrogels, pure fibrin, $Fib_{1.5}D_5$, $Fib_{1.5}D_{7.5}$, and $Fib_{1.5}D_{10}$ in swollen state, and pre-stained fibrinogen (Alexa Fluor-488 dye) was used for hydrogel synthesis and visualized by two-photon laser scanning microscopy (Figure 7). A pure fibrin hydrogel is shown as a reference, which forms a dense fiber structure. In contrast, all fibrin−dextran-MA hydrogels are arranged less dense, as the

https://doi.org/10.1021/acs.biomac.3c00269
Biomacromolecules 2023, 24, 3972−3984

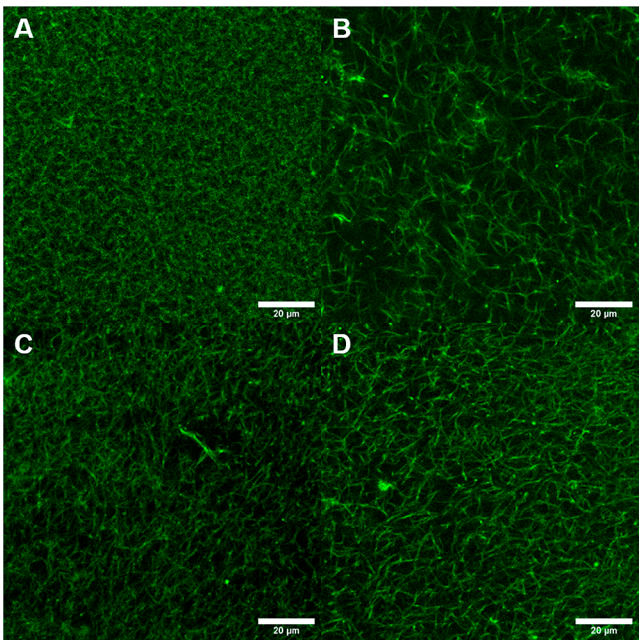

Figure 7. Images of two-photon laser scanning microscopy of stained fibrinogen with Alexa Fluor-488 dye for (A) pure fibrin, (B) $Fib_{1.5}D_5$, (C) $Fib_{1.5}D_{7.5}$, and (D) $Fib_{1.5}D_{10}$.

dextran-MA hydrogel parts are not visualized. In addition, the fibrin fibers are sharp and more oriented compared to the pure fibrin hydrogel. A reason for this could be that the dextran hydrogel compresses the fibrin hydrogel, thus leading to the formation of the fibrin hydrogel between the pores of the dextran hydrogel. This behavior can be seen for all hydrogels with no significant influence of dextran-MA concentration on the formation of fibrin fibers. Further visualization of fibrin−dextran-MA hydrogels with confocal microscopy was conducted for hydrogels with varying fibrin concentration $Fib_{0.7}D_5$, $Fib_{1.5}D$, and $Fib_{4.4}D_5$ (Figure S5).

3.9. Cell Viability Tests. To determine the cytocompatibility of fibrin−dextran-MA hydrogels for the future, as well as the possibility of in vivo applications and the hydrogel's properties as a suitable biomaterial, it is relevant to exclude cytotoxic effects. Therefore, cytotoxicity tests were first performed according to the ISO norm 10993-5. Live/dead staining was performed with L929 mouse fibroblasts and human MSCs, seeded on TCPS (tissue culture polystyrene), fibrin hydrogels, and fibrin−dextran hydrogels.

Cells were cultured for 1, 3, and 7 days and live/dead staining was performed accordingly (Figure 8A). L929 cells showed an increase in cell proliferation when cultured on fibrin gels with and without dextran which can be explained by the softer ECM compared to TCPS provided by the hydrogels. However, morphological changes were observed for L929 mouse fibroblasts when cultured with dextran. On day one, cells appear more roundish on dextran hydrogels compared to hydrogels with fibrin content, but have a fibroblast-like morphology on day three, five and seven. Cells proliferated slower on hydrogels with increased dextran concentrations and grew in cell colonies. L929 fibroblasts that were cultured on $Fib_{1.5}D_{7.5}$ showed the most colony formation over time. Three different MSC donors were compared, and all showed a decreased proliferation and roundish morphology on $Fib_{1.5}D_5$, $Fib_{1.5}D_{10}$, and D_{10} (Figure 8). Many MSCs did grow on $Fib_{1.5}D_{7.5}$ and MSC-like morphology was observed on day 7.

3.10. D-Dimer Human ELISA. The human D-dimer ELISA is implemented to determine the rate of fibrinolysis and to evaluate whether dextran can lead to a deceleration in the degradation process, thus being beneficial by allowing controlled degradation of fibrin-based hydrogels. The results are shown in Figure 9, and the standard curve in Figure S6. Figure 9 illustrates that the addition of different dextran concentrations accounted for a significant decrease in D-dimer concentration after 3 days (between $Fib_{1.5}$ and $Fib_{1.5}D_{10}$). Fibrin hydrogel conditions, which were cultured without dextran featured an overall higher D-dimer concentration ranging from a mean concentration of 474.5 pg mL^{-1} on day 1 to a concentration of 1166.5 pg mL^{-1} after 3 days compared to other compositions. Additionally, the D-dimer concentration decreased with the addition of different dextran concentrations. In this context, compositions containing the highest dextran concentration exhibited the smallest average amount of D-dimers (mean = 122.4 pg mL^{-1}) on day one and an average amount of D-dimers of 230.3 pg mL^{-1} on day three. Hydrogels without fibrin showed almost no D-dimer concentration in the supernatant after one and three days. The evidence indicates that D-dimer concentrations significantly decreased over time in correlation with the addition of higher dextran concentrations.

To summarize the experimental results presented above, an advantage of using the novel fibrin and dextran-MA interpenetrating hydrogel network is that it is possible to easily tune the mechanical properties and to modulate the stiffness of hydrogels through variation of the dextran-MA amounts. In addition, both fibrin and dextran are degradable biopolymers compared to synthetic polymers, e.g., polyethylene oxide or polyethylene glycol.[17,63] In previous studies hyaluronic acid has been mixed with fibrinogen extensively, e.g., by photocrosslinking methacrylate hyaluronic acid.[12,64,65] However, dextran has the advantage of being much more affordable than hyaluronic acid. Furthermore, the usage of dithiols as a crosslinker simplifies the hydrogel preparation, as dithiol present less cytotoxicity than photocrosslinkers and no external factors such as UV light are required. Another novelty presented in this study is the usage of different techniques like microscopy and water NMR diffusometry to determine the mesh size of the bio-based hydrogels. The porosity of hydrogels is an important information for their preselection for cell experiments. So far, the combination of fibrin−dextran-MA hydrogels in cell experiments has not been investigated. However, the group of Liu et al. focused on dextran/gelatin interpenetration networks for the application in vascular TE.[66] Their hydrogels combined the unique properties of polysaccharides and proteins to mimic the ECM. Gelatin, like other ECM proteins, such as collagen or fibrin, which was used in our study, is capable of promoting cell adhesion and proteolytic degradation. Control of the physical and degradation properties of gelatin is limited, which can lead to premature matrix breakdown due to the release of cell-secreted matrix metalloproteinases. With our recent finding of a controllable degradation behavior of fibrin−dextran-MA hydrogels, we eliminated these limits and combined the favorable properties of fibrin and dextran for TE applications.

4. CONCLUSIONS

We synthesized and investigated fibrin−dextran-MA interpenetrating hydrogel networks as a potential biomaterial for TE applications. These fibrin−dextran-MA hydrogels exhibit

https://doi.org/10.1021/acs.biomac.3c00269
Biomacromolecules 2023, 24, 3972−3984

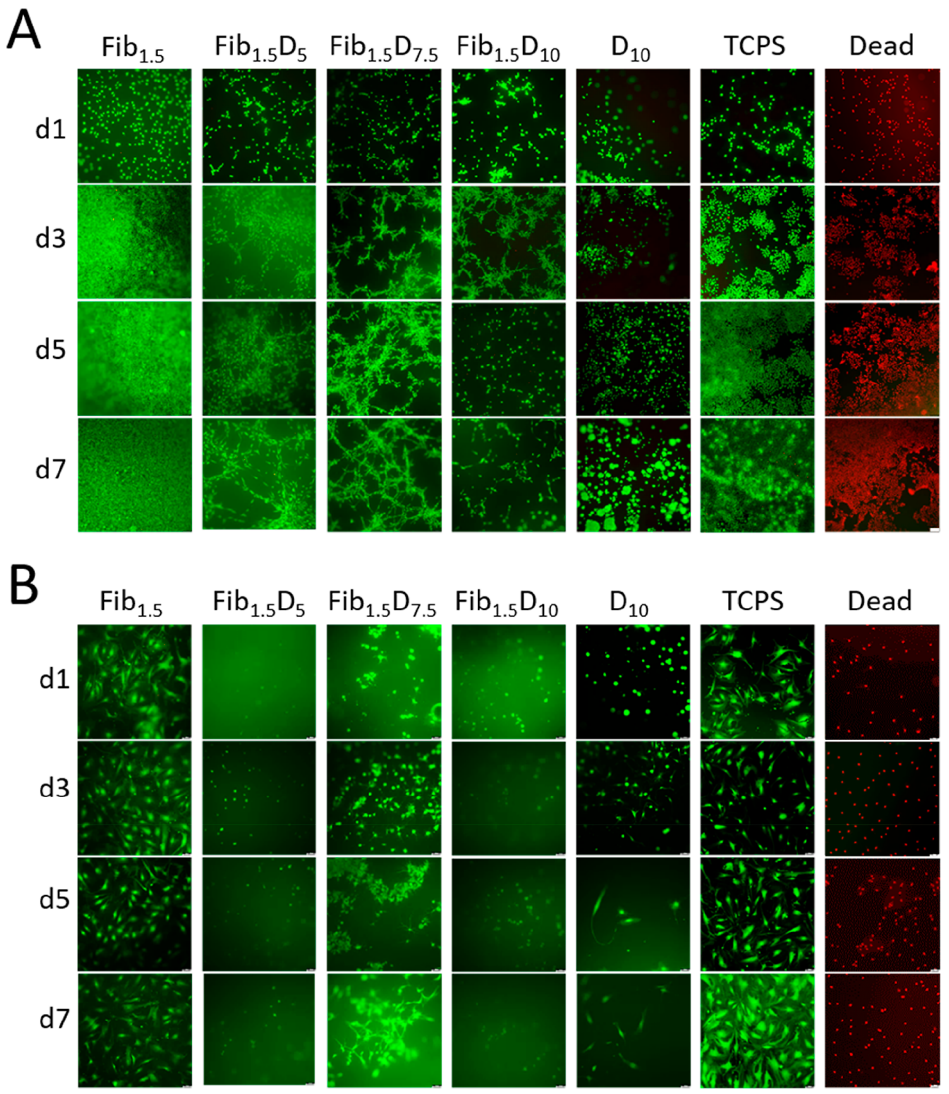

Figure 8. Cytotoxicity test of fibrin/dextran hydrogels in combination with different dextran concentrations according to ISO 10993-5. (A) L929 cells and (B) MSCs were seeded on top of the hydrogels and cultured for 1, 3, and 7 days. Live/dead stainings demonstrate viable cells by green fluorescence and dead cells by red fluorescence.

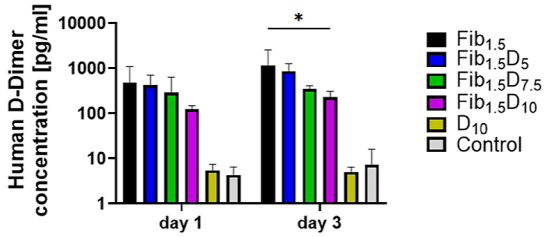

Figure 9. Human D-dimer ELISA to evaluate the influence of dextran on fibrin degradation. The assay was performed after 1 and 3 days with human MSCs cultured on different hydrogel compositions without tranexamic acid. The results illustrate a significant decrease in the concentrations of D-dimers ($p^* < 0.05$) after 3 days between pure fibrin ($Fib_{1.5}$) and fibrin-dextran ($Fib_{1.5}D_{10}$). The amount of D-dimers decreased in correlation with an increasing dextran concentration. Pure dextran (D_{10}) and TCPS show almost no D-dimers in the supernatant.

tunable mechanical properties that are influenced by variation of dextran-MA, fibrinogen, and cross linker amounts. Microscopy images revealed that these hydrogels exhibit a combined structure of typical fibrin and dextran-MA hydrogels with thicker fiber structures in a dense pore structure. Swelling experiments and NMR diffusometry showed the influence of dextran-MA concentrations on the absorbance and mesh sizes of the hydrogels. Two-photon images showed a transition of the fibers from undefined and dense formation in pure fibrin with sharp and oriented fibers in fibrin−dextran-MA hydrogels. The fibrin−dextran hydrogels showed good cytocompatibility and directional cell proliferation along the fibrin parts of the hydrogels. Furthermore, the slower degradation of the hydrogel blends can be achieved compared to pure fibrin hydrogels. By combining the fibrin and dextran-MA hydrogel systems, advanced hydrogels with tunable mechanical properties, slower degradation rate and cytocompatible behavior are obtained; thus, making fibrin−dextran hydrogels suitable and promising candidates as scaffolds in TE applications.

■ ASSOCIATED CONTENT

Supporting Information

The Supporting Information is available free of charge at https://pubs.acs.org/doi/10.1021/acs.biomac.3c00269.

https://doi.org/10.1021/acs.biomac.3c00269
Biomacromolecules 2023, 24, 3972−3984

FT-IR of dextran and dextran-MA; ^{1}H NMR of dextran and dextran-MA; fiber thickness determined form SEM images of fibrin and dextran-MA hydrogels; NMR diffusometry of normalized water diffusivity for fibrin, dextran-MA and fibrin−dextran-MA hydrogels; Young modulus of hydrogels; confocal images of hydrogels with varying fibrin amounts; standard curve of human D-dimer ELISA; and table of p^* for storage modulus of all hydrogels (PDF)

AUTHOR INFORMATION

Corresponding Authors

Sabine Neuss − *Helmholtz Institute for Biomedical Engineering, BioInterface Group, RWTH Aachen University, Aachen 52074, Germany; Institute of Pathology, RWTH Aachen University, Aachen 52074, Germany*; Email: sneuss-stein@ukaachen.de

Andrij Pich − *DWI-Leibniz Institute for Interactive Materials, RWTH Aachen University, Aachen 52074, Germany; Institute for Technical and Macromolecular Chemistry, RWTH Aachen University, Aachen 52074, Germany*; orcid.org/0000-0003-1825-7798; Email: pich@dwi.rwth-aachen.de

Authors

Shannon Anna Jung − *DWI-Leibniz Institute for Interactive Materials, RWTH Aachen University, Aachen 52074, Germany; Institute for Technical and Macromolecular Chemistry, RWTH Aachen University, Aachen 52074, Germany*; orcid.org/0009-0006-3148-9787

Hanna Malyaran − *Helmholtz Institute for Biomedical Engineering, BioInterface Group, RWTH Aachen University, Aachen 52074, Germany; Interdisciplinary Centre for Clinical Research, RWTH Aachen University, Aachen 52074, Germany*

Dan Eugen Demco − *DWI-Leibniz Institute for Interactive Materials, RWTH Aachen University, Aachen 52074, Germany*; orcid.org/0000-0003-0217-5456

Anna Manukanc − *DWI-Leibniz Institute for Interactive Materials, RWTH Aachen University, Aachen 52074, Germany; Institute for Technical and Macromolecular Chemistry, RWTH Aachen University, Aachen 52074, Germany*; orcid.org/0000-0002-1370-7676

Leonie Sophie Häser − *DWI-Leibniz Institute for Interactive Materials, RWTH Aachen University, Aachen 52074, Germany; Institute for Technical and Macromolecular Chemistry, RWTH Aachen University, Aachen 52074, Germany*

Vytautas Kučikas − *Institute for Molecular Cardiovascular Research (IMCAR), RWTH Aachen University, Aachen 52074, Germany*

Marc van Zandvoort − *Institute for Molecular Cardiovascular Research (IMCAR), RWTH Aachen University, Aachen 52074, Germany; Department of Genetics and Cell Biology, GROW, CARIM, MHeNS, Maastricht University, Maastricht 6200 MD, The Netherlands*

Complete contact information is available at: https://pubs.acs.org/10.1021/acs.biomac.3c00269

Author Contributions

$^{\nabla}$S.A.J. and H.M. are shared first authors. S.A.J., H.M., S.N., and A.P. contributed equally to this work. D.E.D. performed NMR diffusometry measurement and analyzed the resulting data. V.K. performed two-photon laser scanning microscopy sample preparation and image acquisition. A.M. and L.S.H. synthesized dextran-MA, performed preliminary experiments and analyzed the resulting data.

Notes

The authors declare no competing financial interest.

ACKNOWLEDGMENTS

This work was supported by the Deutsche Forschungsgemeinschaft (DFG) in the framework of the joint project "Toward a model-based control of biohybrid implant maturation" (PAK961) by the grant NE1650/4-2 and PI614/13-2 and the Excellence Strategy of the Federal Government and the Länder by the grant G:(DE-82)EXS-SF-OPSF761. Additionally, S.A.J. thanks Thomke M. Belthle and Miriam A. Al Enezy-Ulbrich for reviewing the manuscript. Finally, we thank Training Network Aachen-Osaka RECONNECT.

REFERENCES

(1) Doblado, L. R.; Martínez-Ramos, C.; Pradas, M. M. Biomaterials for Neural Tissue Engineering. *Front. Nanotechnol.* **2021**, *3*, 643507.

(2) Janmey, P. A.; Winer, J. P.; Weisel, J. W. Fibrin Gels and Their Clinical and Bioengineering Applications. *J. R. Soc., Interface* **2009**, *6*, 1−10.

(3) Bashir, S.; Hina, M.; Iqbal, J.; Rajpar, A. H.; Mujtaba, M. A.; Alghamdi, N. A.; Wageh, S.; Ramesh, K.; Ramesh, S. Fundamental Concepts of Hydrogels: Synthesis, Properties, and Their Applications. *Polymers (Basel)* **2020**, *12*, 2702.

(4) Ahmed, T. A. E.; Griffith, M.; Hincke, M. Characterization and Inhibition of Fibrin Hydrogel-Degrading Enzymes during Development of Tissue Engineering Scaffolds. *Tissue Eng.* **2007**, *13*, 1469−1477.

(5) Lee, A.; Hudson, A. R.; Shiwarski, D. J.; Tashman, J. W.; Hinton, T. J.; Yerneni, S.; Bliley, J. M.; Campbell, P. G.; Feinberg, A. W. 3D Bioprinting of Collagen to Rebuild Components of the Human Heart. *Science* **2019**, *365*, 482−487.

(6) Liu, Y.; Chan-Park, M. B. Hydrogel Based on Interpenetrating Polymer Networks of Dextran and Gelatin for Vascular Tissue Engineering. *Biomaterials* **2009**, *30*, 196−207.

(7) Baldwin, A. D.; Kiick, K. L. Polysaccharide-Modified Synthetic Polymeric Biomaterials. *Biopolymers* **2010**, *94*, 128−140.

(8) Kang, S. W.; Kim, J. S.; Park, K. S.; Cha, B. H.; Shim, J. H.; Kim, J. Y.; Cho, D. W.; Rhie, J. W.; Lee, S. H. Surface Modification with Fibrin/Hyaluronic Acid Hydrogel on Solid-Free Form-Based Scaffolds Followed by BMP-2 Loading to Enhance Bone Regeneration. *Bone* **2011**, *48*, 298−306.

(9) Dhingra, S.; Weisel, R. D.; Li, R. K. Synthesis of Aliphatic Polyester Hydrogel for Cardiac Tissue Engineering. *Methods Mol. Biol.* **2014**, *1181*, 51−59.

(10) Lin, C. C.; Anseth, K. S. PEG Hydrogels for the Controlled Release of Biomolecules in Regenerative Medicine. *Pharm. Res.* **2009**, *26*, 631−643.

(11) Gsib, O.; Duval, J. L.; Goczkowski, M.; Deneufchatel, M.; Fichet, O.; Larreta-Garde, V.; Bencherif, S. A.; Egles, C. Evaluation of Fibrin-Based Interpenetrating Polymer Networks as Potential Biomaterials for Tissue Engineering. *Nanomaterials* **2017**, *7*, 436.

(12) Zhang, Y.; Heher, P.; Hilborn, J.; Redl, H.; Ossipov, D. A. Hyaluronic Acid-Fibrin Interpenetrating Double Network Hydrogel Prepared in Situ by Orthogonal Disulfide Cross-Linking Reaction for Biomedical Applications. *Acta Biomater.* **2016**, *38*, 23−32.

(13) Pescosolido, L.; Schuurman, W.; Malda, J.; Matricardi, P.; Alhaique, F.; Coviello, T.; Van Weeren, P. R.; Dhert, W. J. A.; Hennink, W. E.; Vermonden, T. Hyaluronic Acid and Dextran-Based Semi-IPN Hydrogels as Biomaterials for Bioprinting. *Biomacromolecules* **2011**, *12*, 1831−1838.

(14) Vorwald, C. E.; Gonzalez-Fernandez, T.; Joshee, S.; Sikorski, P.; Leach, J. K. Tunable Fibrin-Alginate Interpenetrating Network Hydrogels to Support Cell Spreading and Network Formation. *Acta Biomater.* **2020**, *108*, 142−152.
(15) Shivashankar, M.; Mandal, B. K. A Review on Interpenetrating Polymer Network. *Int. J. Pharm. Pharm. Sci.* **2012**, *4*, 1−7.
(16) Zhang, X.; Yang, Y.; Yao, J.; Shao, Z.; Chen, X. Strong Collagen Hydrogels by Oxidized Dextran Modification. *ACS Sustainable Chem. Eng.* **2014**, *2*, 1318−1324.
(17) Dikovsky, D.; Bianco-Peled, H.; Seliktar, D. The Effect of Structural Alterations of PEG-Fibrinogen Hydrogel Scaffolds on 3-D Cellular Morphology and Cellular Migration. *Biomaterials* **2006**, *27*, 1496−1506.
(18) Benavides, O. M.; Quinn, J. P.; Pok, S.; Petsche Connell, J.; Ruano, R.; Jacot, J. G. Capillary-like Network Formation by Human Amniotic Fluid-Derived Stem Cells within Fibrin/Poly(Ethylene Glycol) Hydrogels. *Tissue Eng., Part A* **2015**, *21*, 1185−1194.
(19) Kim, J. A.; An, Y. H.; Yim, H. G.; Han, W. J.; Park, Y. B.; Park, H. J.; Kim, M. Y.; Jang, J.; Koh, R. H.; Kim, S. H.; Hwang, N. S.; Ha, C. W. Injectable Fibrin/Polyethylene Oxide Semi-IPN Hydrogel for a Segmental Meniscal Defect Regeneration. *Am. J. Sports Med.* **2021**, *49*, 1538−1550.
(20) Mosesson, M. W. Fibrinogen and Fibrin Structure and Functions. *J. Thromb. Haemostasis* **2005**, *3*, 1894−1904.
(21) Zhao, H.; Ma, L.; Zhou, J.; Mao, Z.; Gao, C.; Shen, J. Fabrication and Physical and Biological Properties of Fibrin Gel Derived from Human Plasma. *Biomed. Mater.* **2008**, *3*, 015001.
(22) Weisel, J. W. Fibrinogen and Fibrin. *Adv. Protein Chem.* **2005**, *70*, 247−299.
(23) Kattula, S.; Byrnes, J. R.; Wolberg, A. S. Fibrinogen and Fibrin in Hemostasis and Thrombosis. *Arterioscler., Thromb., Vasc. Biol.* **2017**, *37*, e13−e21.
(24) Kurniawan, N. A.; Van Kempen, T. H. S.; Sonneveld, S.; Rosalina, T. T.; Vos, B. E.; Jansen, K. A.; Peters, G. W. M.; Van De Vosse, F. N.; Koenderink, G. H. Buffers Strongly Modulate Fibrin Self-Assembly into Fibrous Networks. *Langmuir* **2017**, *33*, 6342−6352.
(25) Shpichka, A.; Osipova, D.; Efremov, Y.; Bikmulina, P.; Kosheleva, N.; Lipina, M.; Bezrukov, E. A.; Sukhanov, R. B.; Solovieva, A. B.; Vosough, M.; Timashev, P. Fibrin-Based Bioinks: New Tricks from an Old Dog. *Int. J. Bioprint.* **2020**, *6*, 269.
(26) Roska, F. J.; Ferry, J. D. Studies of Fibrin Film. I. Stress Relaxation and Birefringence. *Biopolymers* **1982**, *21*, 1811−1832.
(27) Takada, A.; Makino, Y.; Takada, Y. Effects of Tranexamic Acid on Fibrinolysis, Fibrinogenolysis and Amidolysis. *Thromb. Res.* **1986**, *42*, 39−47.
(28) Chan, L. W.; Wang, X.; Wei, H.; Pozzo, L. D.; White, N. J.; Pun, S. H. A synthetic fibrin cross-linking polymer for modulating clot properties and inducing hemostasis. *Sci. Transl. Med.* **2015**, *7*, 277ra29.
(29) Al Enezy-Ulbrich, M. A.; Malyaran, H.; de Lange, R. D.; Labude, N.; Plum, R.; Rütten, S.; Terefenko, N.; Wein, S.; Neuss, S.; Pich, A. Impact of Reactive Amphiphilic Copolymers on Mechanical Properties and Cell Responses of Fibrin-Based Hydrogels. *Adv. Funct. Mater.* **2020**, *30*, 2003528.
(30) Díaz-Montes, E. Dextran: Sources, Structures, and Properties. *Polysaccharides* **2021**, *2*, 554−565.
(31) Sun, G.; Mao, J. J. Engineering Dextran-Based Scaffolds for Drug Delivery and Tissue Repair. *Nanomedicine* **2012**, *7*, 1771−1784.
(32) Nonsuwan, P.; Matsugami, A.; Hayashi, F.; Hyon, S. H.; Matsumura, K. Controlling the Degradation of an Oxidized Dextran-Based Hydrogel Independent of the Mechanical Properties. *Carbohydr. Polym.* **2019**, *204*, 131−141.
(33) Liu, Z. Q.; Wei, Z.; Zhu, X. L.; Huang, G. Y.; Xu, F.; Yang, J. H.; Osada, Y.; Zrínyi, M.; Li, J. H.; Chen, Y. M. Dextran-Based Hydrogel Formed by Thiol-Michael Addition Reaction for 3D Cell Encapsulation. *Colloids Surf., B* **2015**, *128*, 140−148.
(34) van Dijk-Wolthuis, W. N. E.; Franssen, O.; Talsma, H.; van Steenbergen, M. J.; Kettenes-van den Bosch, J. J.; Hennink, W. E. Synthesis, Characterization, and Polymerization of Glycidyl Methacrylate Derivatized Dextran. *Macromolecules* **1995**, *28*, 6317−6322.
(35) Zhang, R.; Tang, M.; Bowyer, A.; Eisenthal, R.; Hubble, J. A Novel PH- and Ionic-Strength-Sensitive Carboxy Methyl Dextran Hydrogel. *Biomaterials* **2005**, *26*, 4677−4683.
(36) Lix, K.; Tran, M. V.; Massey, M.; Rees, K.; Sauvé, E. R.; Hudson, Z. M.; Algar, W. R. Dextran Functionalization of Semiconducting Polymer Dots and Conjugation with Tetrameric Antibody Complexes for Bioanalysis and Imaging. *ACS Appl. Bio Mater.* **2020**, *3*, 432−440.
(37) Choi, R.; Yang, J.; Choi, J.; Lim, E. K.; Kim, E.; Suh, J. S.; Huh, Y. M.; Haam, S. Thiolated Dextran-Coated Gold Nanorods for Photothermal Ablation of Inflammatory Macrophages. *Langmuir* **2010**, *26*, 17520−17527.
(38) Peng, K.; Tomatsu, I.; Van Den Broek, B.; Cui, C.; Korobko, A. V.; Van Noort, J.; Meijer, A. H.; Spaink, H. P.; Kros, A. Dextran Based Photodegradable Hydrogels Formed via a Michael Addition. *Soft Matter* **2011**, *7*, 4881−4887.
(39) Boyer, M. H.; Shainoff, J. R.; Ratnoff, O. D. Acceleration of Fibrin Polymerization by Calcium Ions. *Blood* **1972**, *39*, 382−387.
(40) Stejskal, E. O.; Tanner, J. E. Spin Diffusion Measurements: Spin Echoes in the Presence of a Time-Dependent Field Gradient. *J. Chem. Phys.* **1965**, *42*, 288−292.
(41) Callaghan, P. T. *Translational Dynamics and Magnetic Resonance: Principles of Pulsed Gradient Spin Echo NMR*; Oxford University Press, 2011.
(42) Kimmich, R. *NMR, Tomography, Diffusometry, Relaxometry*, 1st ed.; Springer: Berlin, Heidelberg, 1997.
(43) Price, W. S. *NMR Studies of Translational Motion*; Cambridge University Press, 2009.
(44) Pittenger, M. F.; Mackay, A. M.; Beck, S. C.; Jaiswal, R. K.; Douglas, R.; Mosca, J. D.; Moorman, M. A.; Simonetti, D. W.; Craig, S.; Marshak, D. R. Multilineage Potential of Adult Human Mesenchymal Stem Cells. *Science* **1999**, *284*, 143−147.
(45) Haynesworth, S. E.; Goshima, J.; Goldberg, V. M.; Caplan, A. I. Characterization of Cells with Osteogenic Potential from Human Marrow. *Bone* **1992**, *13*, 81−88.
(46) Neuss, S.; Apel, C.; Buttler, P.; Denecke, B.; Dhanasingh, A.; Ding, X.; Grafahrend, D.; Groger, A.; Hemmrich, K.; Herr, A.; Jahnen-Dechent, W.; Mastitskaya, S.; Perez-Bouza, A.; Rosewick, S.; Salber, J.; Wöltje, M.; Zenke, M. Assessment of Stem Cell/Biomaterial Combinations for Stem Cell-Based Tissue Engineering. *Biomaterials* **2008**, *29*, 302−313.
(47) Liu, Z. Q.; Wei, Z.; Zhu, X. L.; Huang, G. Y.; Xu, F.; Yang, J. H.; Osada, Y.; Zrínyi, M.; Li, J. H.; Chen, Y. M. Dextran-Based Hydrogel Formed by Thiol-Michael Addition Reaction for 3D Cell Encapsulation. *Colloids Surf., B* **2015**, *128*, 140−148.
(48) Wedgwood, J.; Freemont, A. J.; Tirelli, N. Rheological and Turbidity Study of Fibrin Hydrogels. *Macromol. Symp.* **2013**, *334*, 117−125.
(49) Hasanzadeh, E.; Mahmoodi, N.; Basiri, A.; Esmaeili Ranjbar, F.; Hassannejad, Z.; Ebrahimi-Barough, S.; Azami, M.; Ai, J.; Rahimi-Movaghar, V. Proanthocyanidin as a Crosslinking Agent for Fibrin, Collagen Hydrogels and Their Composites with Decellularized Wharton's-Jelly-Extract for Tissue Engineering Applications. *J. Bioact. Compat. Polym.* **2020**, *35*, 554−571.
(50) Blomback, B.; Procyk, R.; Adamson, L.; Hessel, B. FXIII Induced Gelation of Human Fibrinogen—An Alternative Thiol Enhanced, Thrombin Independent Pathway. *Thromb. Res.* **1985**, *37*, 613−627.
(51) Piechocka, I. K.; Bacabac, R. G.; Potters, M.; Mackintosh, F. C.; Koenderink, G. H. Structural Hierarchy Governs Fibrin Gel Mechanics. *Biophys. J.* **2010**, *98*, 2281−2289.
(52) Gao, Y.; Cho, H. J. Correction: Quantifying the Trade-off between Stiffness and Permeability in Hydrogels. *Soft Matter* **2022**, *18*, 8906.
(53) Richbourg, N. R.; Peppas, N. A. The Swollen Polymer Network Hypothesis: Quantitative Models of Hydrogel Swelling, Stiffness, and Solute Transport. *Prog. Polym. Sci.* **2020**, *105*, 101243.

https://doi.org/10.1021/acs.biomac.3c00269
Biomacromolecules 2023, 24, 3972−3984

(54) Richbourg, N. R.; Wancura, M.; Gilchrist, A. E.; Toubbeh, S.; Harley, B. A. C.; Cosgriff-Hernandez, E.; Peppas, N. A. Precise Control of Synthetic Hydrogel Network Structure via Linear, Independent Synthesis-Swelling Relationships. *Sci. Adv.* **2021**, *7*, 3245−3257.
(55) Ryan, E. A.; Mockros, L. F.; Weisel, J. W.; Lorand, L. Structural Origins of Fibrin Clot Rheology. *Biophys. J.* **1999**, *77*, 2813−2826.
(56) Ferri, F.; Greco, M.; Arcävito, G.; De Spirito, M.; Rocco, M. Structure of Fibrin Gels Studied by Elastic Light Scattering Techniques: Dependence of Fractal Dimension, Gel Crossover Length, Fiber Diameter, and Fiber Density on Monomer Concentration. *Phys. Rev. E: Stat., Nonlinear, Soft Matter Phys.* **2002**, *66*, 011913.
(57) Williams, J. C.; Mark, L. A.; Eichholtz, S. Partition and Permeation of Dextran in Polyacrylamide Gel. *Biophys. J.* **1998**, *75*, 493−502.
(58) Amsden, B. G. Hydrogel Mesh Size and Its Impact on Predictions of Mathematical Models of the Solute Diffusion Coefficient. *Macromolecules* **2022**, *55*, 8399−8408.
(59) Hadjiev, N. A.; Amsden, B. G. An Assessment of the Ability of the Obstruction-Scaling Model to Estimate Solute Diffusion Coefficients in Hydrogels. *J. Controlled Release* **2015**, *199*, 10−16.
(60) Richbourg, N. R.; Ravikumar, A.; Peppas, N. A. Solute Transport Dependence on 3D Geometry of Hydrogel Networks. *Macromol. Chem. Phys.* **2021**, *222*, 2100138.
(61) Li, Z.; Yu, C.; Kumar, H.; He, X.; Lu, Q.; Bai, H.; Kim, K.; Hu, J. The Effect of Crosslinking Degree of Hydrogels on Hydrogel Adhesion. *Gels (Basel, Switzerland)* **2022**, *8*, 682.
(62) Khan, S.; Ranjha, N. M. Effect of Degree of Cross-Linking on Swelling and on Drug Release of Low Viscous Chitosan/Poly(Vinyl Alcohol) Hydrogels. *Polym. Bull.* **2014**, *71*, 2133−2158.
(63) Akpalo, E.; Bidault, L.; Boissière, M.; Vancaeyzeele, C.; Fichet, O.; Garde, V. L. Fibrin-Polyethylene Oxide Interpenetrating Polymer Networks: New Self-Supported Biomaterials Combining the Properties of Both Protein Gel and Synthetic Polymer. *Acta Biomater.* **2011**, *7*, 2418−2427.
(64) Tavsanli, B.; Can, V.; Okay, O. Mechanically Strong Triple Network Hydrogels Based on Hyaluronan and Poly(N,N-Dimethylacrylamide). *Soft Matter* **2015**, *11*, 8517−8524.
(65) Storozhylova, N.; Crecente-Campo, J.; Cabaleiro, D.; Lugo, L.; Dussouy, C.; Simões, S.; Monteiro, M.; Grandjean, C.; Alonso, M. J. An In Situ Hyaluronic Acid-Fibrin Hydrogel Containing Drug-Loaded Nanocapsules for Intra-Articular Treatment of Inflammatory Joint Diseases. *Regener. Eng. Transl. Med.* **2020**, *6*, 201−216.
(66) Liu, Y.; Chan-Park, M. B. Hydrogel Based on Interpenetrating Polymer Networks of Dextran and Gelatin for Vascular Tissue Engineering. *Biomaterials* **2009**, *30*, 196−207.

https://doi.org/10.1021/acs.biomac.3c00269
Biomacromolecules 2023, 24, 3972−3984